ACS chemical biology

Articles

Cite This: ACS Chem. Biol. 2019, 14, 934−940

pubs.acs.org/acschemicalbiology

A Nonaggregating Heptamethine Cyanine for Building Brighter Labeled Biomolecules

Michael P. Luciano,[†] Stephen N. Crooke,[‡] Saghar Nourian,[†] Ivan Dingle,[†] Roger R. Nani,[†] Gabriel Kline,[†] Nimit L. Patel,[§] Christina M. Robinson,[∥] Simone Difilippantonio,[∥] Joseph D. Kalen,[§] M. G. Finn,[‡] and Martin J. Schnermann*[,†]

[†]Chemical Biology Laboratory, Center for Cancer Research, National Cancer Institute, Frederick, Maryland 21702, United States

[‡]School of Chemistry and Biochemistry, School of Biological Sciences, Georgia Institute of Technology, 901 Atlantic Drive, Atlanta, Georgia 30332, United States

[§]Small Animal Imaging Program, Frederick National Laboratory for Cancer Research, Leidos Biomedical Research Inc., Frederick, Maryland 21702, United States

[∥]Animal Research Technical Support, Frederick National Laboratory for Cancer Research, Leidos Biomedical Research Inc., Frederick, Maryland 21702, United States

Supporting Information

ABSTRACT: Heptamethine cyanines are broadly used for a range of near-infrared imaging applications. As with many fluorophores, these molecules are prone to forming nonemissive aggregates upon biomolecule conjugation. Prior work has focused on persulfonation strategies, which only partially address these issues. Here, we report a new set of peripheral substituents, short polyethylene glycol chains on the indolenine nitrogens and a substituted alkyl ether at the C4′ position, that provide exceptionally aggregation-resistant fluorophores. These symmetrical molecules are net-neutral, can be prepared in a concise sequence, and exhibit no evidence of H-aggregation even at high labeling density when appended to monoclonal antibodies or virus-like particles. The resulting fluorophore−biomolecule conjugates exhibit exceptionally bright *in vitro* and *in vivo* signals when compared to a conventional persulfonated heptamethine cyanine. Overall, these efforts provide a new class of heptamethine cyanines with significant utility for complex labeling applications.

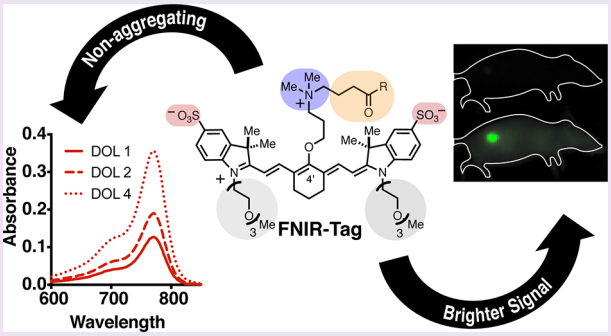

Near-infrared (NIR) wavelengths can facilitate the visualization of biological processes in complex organismal settings. The use of fluorophore-labeled biomacromolecules is an enduring strategy employed across the spectrum of fundamental to applied biomedical science.[1,2] However, fluorophore conjugation often alters the properties of both the fluorophore and the molecule to which it is attached.[3] Specifically, important parameters such as brightness, target binding, *in vivo* stability, and pharmacokinetics (PK) are often impacted.[4−7] An important component of these issues is the formation of dye aggregates. In particular, H-aggregates, which are characterized by the appearance of a hypsochromic (blue-shifted) absorption band and a reduction in fluorescence intensity, are a common consequence of fluorophore bioconjugation.[3,8]

The most common strategy to avoid aggregation, pioneered with the "Cy" dyes, is the introduction of multiple anionic sulfonate groups.[9−11] This broadly adopted strategy has led to extensively used commercial dyes, including Licor's IR-Dye800CW (IR-800CW, Figure 1A).[11] Notably, IR-800CW conjugates of the anti-EGFR antibody, panitumumab, and the small molecule, folate, are advancing through various clinical trials for fluorescence-guided surgical excision of solid tumors.[12−14] However, while dye sulfonation is a highly successful strategy in the visible range, persulfonated NIR fluorophores are still prone to the formation of aggregates at even moderate labeling density. Because NIR fluorophores are intrinsically less emissive than their counterparts in the visible range, strategies to circumvent the formation of nonemissive aggregates are a pressing need.

Our approach to develop cyanine fluorophores for emerging imaging applications has been to identify novel chemical strategies that directly modify the core chromophore unit.[15−17] Relevant to these studies, we developed a general chemical strategy to modify the C4′ position of the heptamethine scaffold with an *O*-alkyl group.[18] These molecules are formed through an electrophile-integrating *N*- to *O*-rearrangement reaction from the corresponding readily available C4′ amino

Received: February 14, 2019
Accepted: April 10, 2019
Published: April 27, 2019

DOI: 10.1021/acschembio.9b00122
ACS Chem. Biol. 2019, 14, 934−940

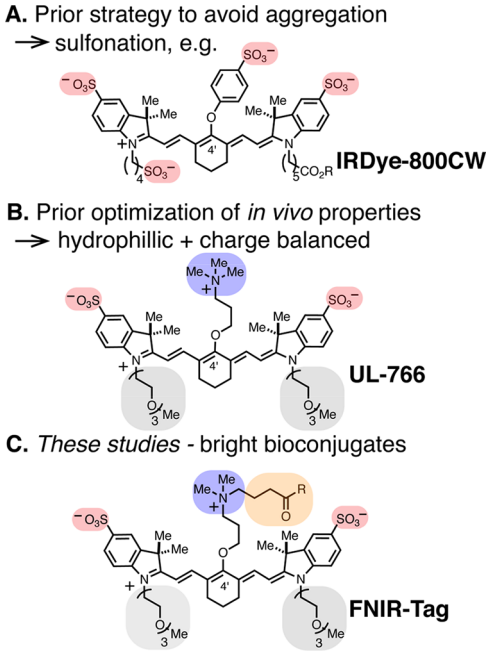

Figure 1. Prior strategies to improve heptamethine cyanine aggregation (A), efforts to improve their *in vivo* properties (B), and studies reported here (C).

precursors. Significantly, the extensively studied C4′-*O*-aryl (e.g., IR-800CW) and related compounds form C4′-thio adducts upon exposure to thiol-containing biomolecules, as revealed recently in studies from our lab and others.[19−21] By contrast, these C4′-*O*-alkyl cyanines are resistant to this chemical pathway, circumventing the potential for these adducts to have deleterious effects. This chemistry has been employed to examine the role of substituent patterns on the properties of these molecules and their antibody conjugates.[22,23] For example, we examined the use of tetralkyl ammonium functional groups appended to indolenine nitrogens, a strategy examined productively for small-molecule-fluorophore conjugates.[24−28] However, in the case of antibody conjugates, H-aggregation remained a persistent issue, and the resulting compounds showed improved properties only at modest labeling density.[29]

To improve the properties of heptamethine cyanines for biomolecule labeling applications, we drew on recent studies that led to the identification of UL-766 (Figure 1B).[20] Fluorophores that undergo exclusive renal clearance could enable ready visualization of the ureter, a sensitive duct often injured during abdominal surgery. The compound that emerged for this application following significant screening efforts is the highly water-soluble but net-neutral UL-766. This net-neutral compound contains short ethylene glycol chains at the indolenine nitrogen positions and a trimethylalkylammonium salt at the C4′ position. In the design of these studies, we hypothesized that modification of this scaffold for bioconjugation through the tetraalkylammonium linker might deliver unique properties for biomolecule labeling.

In the report below, we detail the synthesis, characterization, and testing of a novel NIR fluorophore that circumvents the issue of H-aggregation and provides exceptionally bright fluorophore−antibody conjugates at high labeling density. This optimized dye, FNIR-Tag (Figure 1C), can be synthesized in a short, scalable (up to 0.5 g) synthetic sequence and is used here as the NHS ester and alkyne functionalized variants, though others are certainly feasible. Similarly labeled monoclonal antibody (mAb) conjugates of FNIR-Tag show superior tumor localization and brightness when compared with IR-800CW conjugates in an *in vivo* imaging study of mice bearing EGFR+ tumors. FNIR-Tag-mAb conjugates are also less subject to liver uptake than conjugates of IR-800CW. We also evaluated FNIR-Tag conjugates of virus-like particles (VLPs) derived from the bacteriophage Qβ. These conjugates also proved significantly brighter in both cellular and *in vivo* studies. Overall, these studies provide a NIR cyanine with excellent properties for complex, high-density labeling applications.

RESULTS AND DISCUSSION

Synthesis and Photophysical Properties of a Net-Neutral, Bioconjugatable Fluorophore. The synthesis of the FNIR-Tag derivatives from previously described **1** is outlined in Scheme 1.[20] The addition of amine **2** (available in 3 steps from commercial material as described in the Supporting Information) to 4′-chloroheptamethine cyanine **1** in the presence of DIPEA at 120 °C for 25 min provided the deep blue C4′-*N*-linked heptamethine cyanine **3** in 47% yield after reversed-phase purification. In a one-pot process, carboxylic acid **4** was prepared by stirring **3** in neat TFA for 5 min at 60 °C, during which time LC-MS analysis of the reaction indicated both the expected removal of the *t*-butyl ester group and C4′ *N*- to *O*-transposition.[20] After removing the TFA, the mixture was exhaustively alkylated by treatment with excess $NaHCO_3$ and MeI in DMF at 60 °C, resulting in the formation of both the desired carboxylic acid **4** (33%) and the methyl ester **5** in yields of 20−30%. The latter could be saponified by treatment with 1 M NaOH in MeOH:H_2O to

Scheme 1. Synthesis of FNIR-Tag-NHS and FNIR-Tag-alkyne

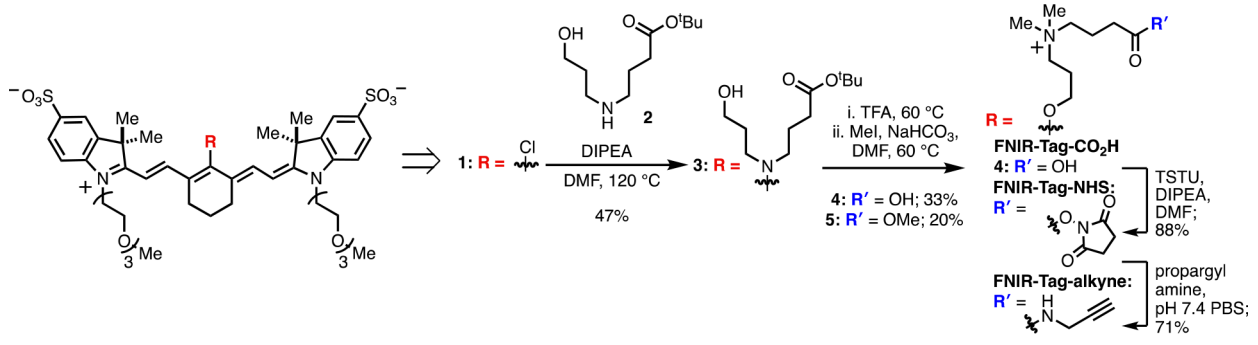

DOI: 10.1021/acschembio.9b00122
ACS Chem. Biol. 2019, 14, 934−940

Table 1. Properties of the Free Dyes Used in This Study in PBS

	λ_{abs} (nm)	λ_{em} (nm)	ε (M^{-1} cm^{-1})	Φ_F (PBS)	$\varepsilon \times \Phi_F$	rel. brightness (PBS)
IR-800CWCO$_2$H	774	795[a]	240 000	0.087	23 490	1.2
FNIR-Tag-CO$_2$H	765	788[b]	200 000	0.099	19 800	1.0

[a] $\lambda_{excitation}$ = 740 nm. [b] $\lambda_{excitation}$ = 730 nm.

provide **4** (see Supporting Information). The carboxylic acid **4**, FNIR-Tag, can be converted to FNIR-Tag-NHS using *N*,*N*,*N*′,*N*′-tetramethyl-*O*-(*N*-succinimidyl)uronium tetrafluoroborate (TSTU) in 88% yield. The conversion of FNIR-Tag-NHS to FNIR-Tag-alkyne was carried out using propargyl amine in 50 mM PBS (pH 7.4) in 71% yield.

Properties of unconjugated FNIR-Tag and IR-800CW carboxylic acids are shown in Table 1. As expected, the C4′ *O*-alkyl cyanine exhibits an absorption/emission maxima (765/788 nm) well in the NIR region that is similar to IR-800CW at 774/795 nm. Both dyes have similar absorption coefficients (ε), absolute quantum yields (Φ_F), and brightness ($\varepsilon \times \Phi_F$) in PBS solution with free IR-800CW being slightly brighter (Table 1). Also as expected, both of the free dyes have similar photostability (Figure S1).

Conjugation of FNIR-Tag with the anti-EGFR mAb panitumumab was carried out in 50 mM PBS (pH 7.4) with molar excesses of 2.2, 4.4, and 8.1 to provide the desired lysine-labeled panitumumab conjugates with degree of labeling (DOL) of 1, 2, and 4 (± 0.2), respectively (Figure 2). We found that NHS-ester labeling proceeds with greater efficiency at pH 7.4 then at pH 8.5, even though the more basic pH is more commonly employed for NHS-ester labeling studies. We attribute this observation to the enhanced chemical reactivity of FNIR-Tag NHS-ester, which perhaps arises from an inductive effect of the electron withdrawing quaternary amine. Similarly labeled samples with IR-800CW (DOL 1, 2, and 4) were obtained by carrying out the labeling using 1 M PBS (pH 8.5). To confirm that the dyes were covalently attached, all samples were purified, incubated at 25 °C for 18 h, and then repurified by size exclusion chromatography (which led to a modest decrease in dye signal, Figure S2). Samples were analyzed by SDS-PAGE to confirm conjugate purity (Figure S3).

The optical properties of these conjugates were analyzed by several methods. The absorption/emission curves are shown in Figure 2A, B (500 nM in protein concentration in 50 mM pH 7.4 PBS). The formation of a significant H-aggregate peak in the absorption spectrum (~705 nm) is apparent with the IR-800CW conjugates even at DOL 1, which worsens at higher DOL of 2 and 4. By contrast, FNIR-Tag does not form a significant H-aggregate band over this range of labeling density. Of note, this trend persists in the presence of serum proteins (Figure S4). The impact of H-aggregation on the fluorescent emission of these conjugates is dramatic. With IR-800CW, the fluorescent emission of the antibody conjugates is nearly constant across the range of labeling density, meaning added fluorophores do not increase brightness of the individual antibody conjugates. By contrast, the emission of FNIR-Tag-panitumumab conjugates increases with higher labeling density. Demonstrating that this effect is the result of H-aggregation, diluting the conjugates in 50:50 MeOH:PBS to denature the protein removes the presence of H-aggregate peak and increases the emission of the conjugates (Figures S5 and S6). The impact of aggregation on emissive properties of these conjugates can also be demonstrated by measuring the

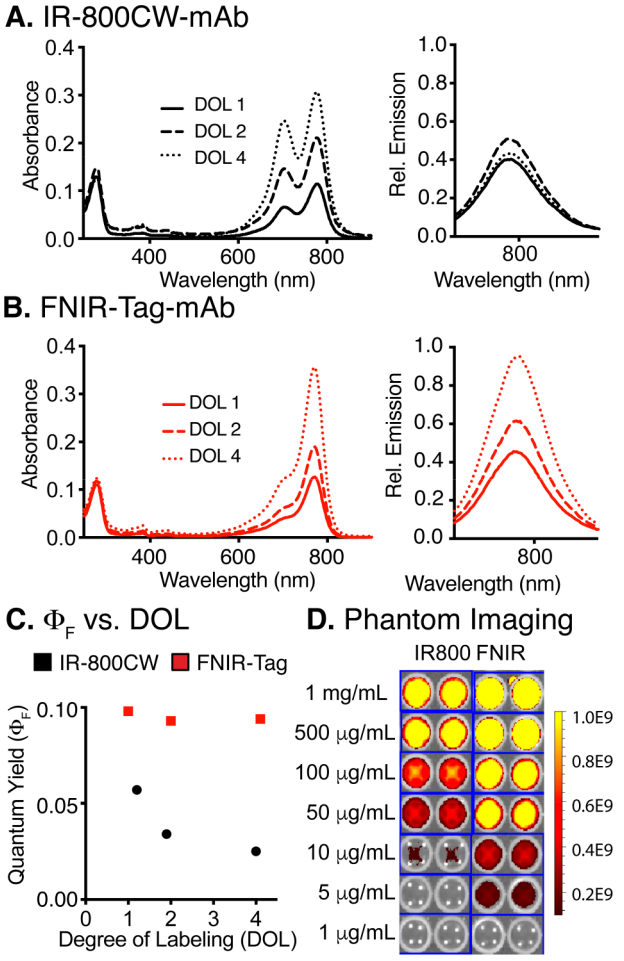

Figure 2. Absorbance and emission spectra of IR-800CW (A) and FNIR-Tag (B) to panitumumab (500 nM) of DOL 1, 2, and 4 conjugates in 50 mM pH 7.4 PBS. (C) Absolute quantum yields of fluorescence (Φ_F) of the panitumumab conjugates (250 nM effective dye concentration) in 50 mM pH 7.4 PBS. (D) Phantom IVIS imaging of DOL4-panitumumab conjugates in 50 mM pH 7.4 PBS. Scale bar represents epi-fluorescent in total radiant efficiency.

absolute quantum yields of fluorescence (Φ_F) of the differentially labeled conjugates. In the case of IR-800CW-antibody conjugates, quantum yield decreases as a function of increased labeling from ~9 to ~2.5%. By contrast, the quantum yield of FNIR-Tag conjugates maintains nearly the same value of the free dye (9−10%) with increasing labeling density. To examine the relative brightness of these conjugates on an *in vivo* imaging system, we carried out phantom imaging on the PerkinElmer IVIS system. In this context, DOL-4 antibody conjugates of FNIR-Tag could be readily visualized at a lower concentration (5 μg/mL) than that required for similarly labeled conjugates of IR-800CW (10−50 μg/mL) (Figure 2D).

Comparison of FNIR-Tag and IR-800CW mAb Conjugates *In Vivo*. The data above suggested that FNIR-Tag-

DOI: 10.1021/acschembio.9b00122
ACS Chem. Biol. 2019, 14, 934−940

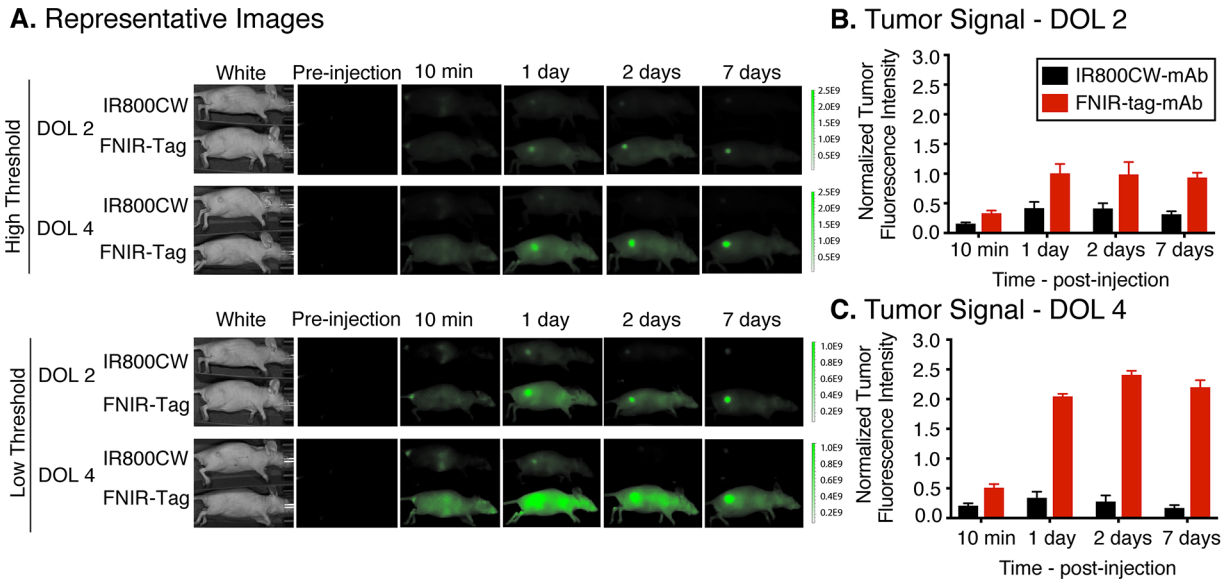

Figure 3. (A) Images of MDA-MB-468 tumor-bearing mice injected with 100 μg of IR-800CW and FNIR-Tag at DOL 2 and 4 conjugates with panitumumab at preinjection and 10 min, 1 day, 2 day, and 7 day time points postinjection. Scale bar represents epi-fluorescent in total radiant efficiency. Tumor signal (total radiant efficiency, all values $\times 10^{10}$) normalized to tumor size for DOL 2 (B) and DOL 4 (C) (all paired columns are statistically significant differences using Student's *t*-test ($p \leq 0.001$)).

mAb conjugates might have favorable fluorescence properties relative to those of IR-800CW *in vivo*. We also speculated that reduced dye aggregation might impact the pharmacokinetics of the mAb conjugates. To compare the two mAb conjugates, *in vivo* imaging was carried out using athymic nude mice bearing EGFR+ tumors implanted in their right flank (n = 5 per group). The mice were injected with 100 μg of either IR-800CW or FNIR-Tag conjugates of panitumumab of DOL 2 or 4. Fluorescence images were recorded before injection and at 10 min, 24 h, 48 h, and 1 week postinjection (Figure 3A and Figure S7). At the peak accumulation of both fluorophores in the tumor (48 h), the radiance output of FNIR-Tag is 2.5X higher at DOL 2 and 7.1X higher at DOL 4. We also noted that at an initial 10 min time point there was significantly higher liver uptake of the IR-800CW than with FNIR-Tag conjugates (Figure S8). However, at this 100 μg dose, the tumor to background (TBR, background taken in the neck region) ratio was indistinguishable during this time course (Figure S9). The latter observation is perhaps not surprising, as this dose was previously optimized for IR-800CW conjugates and not for conjugates of this new brighter dye.

We then carried out a dose lowering study with the goal of defining an optimal dose for FNIR-Tag-mAb conjugates. We chose to examine three doses, 10, 5, and 1 μg, which span the lower end of the doses used in prior studies. We observed clearly discernible signal using FNIR-Tag-mAb conjugates throughout this range, while IR-800CW-mAb tumor signal could not be visualized below 5 μg (Figure S10). In quantifying these images, significantly higher fluorescence intensity was observed in nearly all studies (Figure 4A). Significantly improved TBR was observed for the 10, 5, and 1 μg doses of FNIR-Tag conjugates relative to conjugates IR-800CW starting on day 2 with values reaching 5.78 at day 7 with a 5 μg dose (Figure 4B). Finally, dramatically higher liver to background ratios were observed for the 10 and 5 μg doses of IR-800CW conjugates at 4 h and 1 day time points (Figure 4C). The observation that FNIR-Tag antibody conjugates are less subject to hepatobiliary uptake is likely to be significant

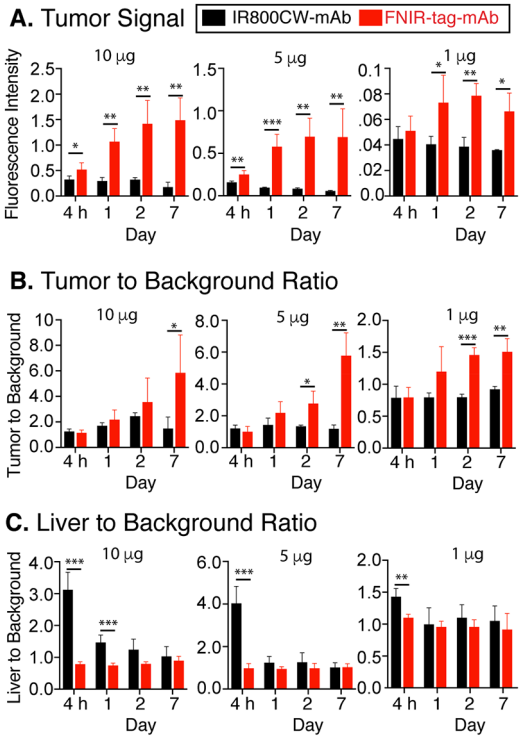

Figure 4. Tumor signal (total radiant efficiency, all values $\times 10^9$) normalized to tumor size (A), tumor to background ratio (B), and liver to background ratio (C) of MDA-MB-468 tumor-bearing mice injected with 10, 5, and 1 μg of IR-800CW and FNIR-Tag DOL 4 conjugates of panitumumab (statistical analysis was performed between groups at the same time point using Student's *t*-test; *$p \leq$ 0.5, **$p \leq 0.01$, ***$p \leq 0.001$).

utility, particularly in instances that seek to visualize biological processes in this region.

Synthesis and Evaluation of Labeled VLPs. We extended our evaluation of FNIR-Tag to conjugates of VLPs

DOI: 10.1021/acschembio.9b00122
ACS Chem. Biol. 2019, 14, 934−940

derived from the bacteriophage Qβ. The Qβ VLP has been explored extensively for applications in vaccinology and drug delivery,[30−33] making it an ideal nanoparticle system for preliminary *in vivo* imaging studies. The multivalent display of lysine residues on the VLP surface[34] allows labeling to be compared at a higher density than possible using mAbs. Similar to the panitumumab conjugates, VLPs labeled with FNIR-Tag show superior brightness and stability when compared with IR-800CW conjugates.

Short azido linkers were installed on the VLPs using standard NHS coupling to make the particles amenable to modification by copper-catalyzed azide−alkyne cycloaddition (CuAAC) chemistry (see Methods in the Supporting Information for details). Conjugation of FNIR-Tag-alkyne with the Qβ-N_3 VLPs, which were prepared as previously described,[34] was carried out via the CuAAC reaction in 100 mM potassium phosphate buffer (pH 7.4) at 50 °C for 3 h with molar equivalents of 0.5, 1, and 2 (relative to azide) to provide conjugates with a staggered degree of labeling (Figure 5; see Methods in the Supporting Information for detailed conjugation conditions). As higher degrees of modification might interfere with particle surface properties, we aimed for fewer than 100 modifications on each particle. Conjugates were prepared with IR-800CW (0.5, 1, and 2 mol eq) under similar conditions (Figure 5). All samples were subsequently purified by centrifugal filtration. Conjugate purity and the absence of free dye were confirmed by absorbance measurements of the supernatant and retentate after each passage (data not shown). Interestingly, higher loadings were achieved with FNIR-Tag (23, 40, and 70 attached dyes) compared to IR-800CW (9, 20, and 33 attached dyes) under all conditions screened. Notably, reaction with 2.0 mol equiv of IR-800CW yielded significant aggregation of the final product, which was not observed under similar conditions with FNIR-Tag (Figure 5B). As a result, loadings higher than 33 ± 3 IR-800CW molecules could not be achieved under these conditions (Figure 5A). Labeling was quantified by relating absorbance measurements (at λ_{abs}) for either FNIR-Tag or IR-800CW with the total protein concentration.

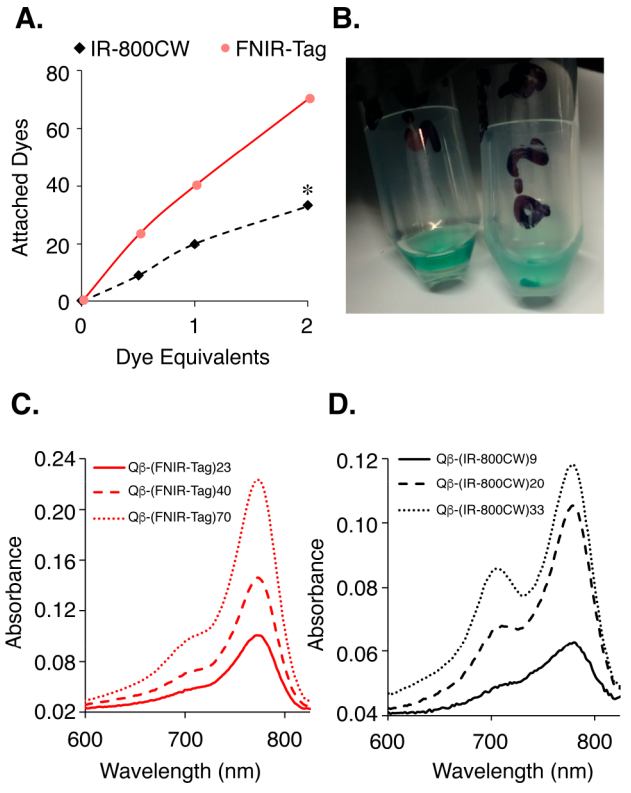

Figure 5. Stability and photophysical properties of VLP-fluorophore conjugates. (A) Quantification of the number of attached fluorophores as a function of molar equivalents added in the CuAAC reaction for FNIR-Tag (blue) and IR-800CW (red). An asterisk (*) indicates conditions where significant particle aggregation was observed. (B) Representative image of the final products from the reactions using 2 mol equiv of fluorophore, demonstrating visible aggregates for particles labeled with IR-800CW (right) but none for those labeled with FNIR-Tag under similar conditions (left). (C and D) Absorbance spectra of VLP conjugates with FNIR-Tag (C) and IR-800CW (D) with increasing degrees of fluorophore modification. All samples were at 20 μg/mL total protein in 100 mM potassium phosphate buffer (pH 7.4).

Absorbance curves for the purified conjugates were obtained following dilution in 100 mM potassium phosphate buffer to yield solutions that were 20 μg/mL in protein. Similar to the antibody conjugates, a significant H-aggregate peak was observed in the absorbance spectrum for IR-800CW conjugates with as few as 20 attached dyes and was significantly worse at higher levels of modification (Figure 5D). No significant H-aggregate band was detected for any of the FNIR-Tag conjugates under these conditions (Figure 5C).

Comparison of FNIR-Tag and IR-800CW VLP Conjugates *in Vitro* and *in Vivo*. We then evaluated VLP-fluorophore conjugate performance both *in vitro* and *in vivo*. To compare the brightness of the conjugates, C166 mouse endothelial cells were incubated with 20 nM VLP at 37 °C for 1 h. Samples were extensively washed to remove VLPs not bound to the cellular surface and subsequently fixed to preserve any interactions prior to analysis by flow cytometry. FNIR-Tag conjugates were significantly brighter than IR-800CW conjugates at similar labeling densities (Figure 6A and B), assuming that cell binding and uptake of the particles is not influenced by the nature of the attached dye. This result is consistent with the data obtained for mAb conjugates (described above). Interestingly, increasing the labeling density of IR-800CW slightly diminished the fluorescence (Figure S11A), whereas the emission of FNIR-Tag conjugates increased with the subsequent addition of fluorophores (Figure S11B). These data further suggest that H-aggregation significantly influences the fluorescence emission of IR-800CW conjugates.

Finally, we conducted an initial comparative imaging study in mice to evaluate the performance of the VLP-fluorophore conjugates *in vivo*. Given the superior brightness of the FNIR-Tag panitumumab conjugates *in vivo* and the stability of Qβ-FNIR-Tag conjugates at high loadings, we speculated that it would be possible to administer a lower dose of VLPs and still achieve sensitive detection by virtue of the greater number of attached fluorophores. Qβ VLPs and other nanoparticle systems are well-known to be cleared from circulation through the reticuloendothelial system and begin to accumulate in the liver within the first hour of administration;[35] therefore, we sought to image accumulation of both FNIR-Tag and IR-800CW conjugates in the livers of naïve CD-1 mice (n = 3 per group) following intravenous administration. Mice were injected with either 50 μg of Qβ-$(IR800CW)_{20}$ or 25 μg of Qβ-$(FNIR\text{-}Tag)_{70}$, and fluorescence images were recorded at 2 and 24 h postinjection (Figure 6C). The attachment of 20 IR-

DOI: 10.1021/acschembio.9b00122
ACS Chem. Biol. 2019, 14, 934−940

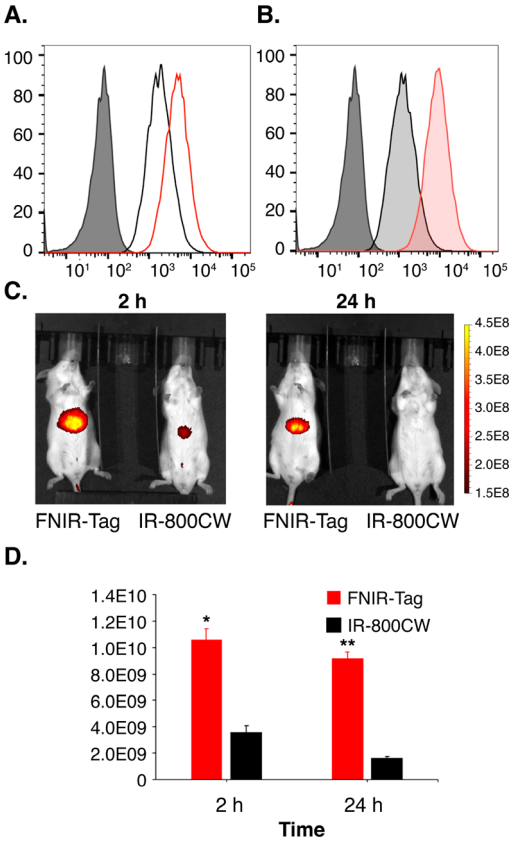

Figure 6. Comparison of VLP conjugate brightness by flow cytometry and whole animal imaging. (A and B) VLP uptake in mouse C166 endothelial cells as measured with conjugates of both FNIR-Tag (red) and IR-800CW (black) at low (A) and high (B) fluorophore loadings. (C) Representative images demonstrating detection of VLP conjugates in the liver at 2 h (left panel) and 24 h (right panel) postinjection. FNIR-Tag = 25 μg dose of Qβ-$(\text{FNIR-Tag})_{70}$; IR-800CW = 50 μg dose of Qβ-$(\text{IR-800CW})_{20}$. Scale bar represents epifluorescent in total radiant efficiency. (D) Quantitative analysis of the fluorescence intensity detected at 2 and 24 h postinjection. Data are mean value ± standard error. Statistical analysis was performed between groups at the same time point using Student's *t*-test. $^*p \leq 0.05$; $^{**}p \leq 0.01$.

800CW dyes to the Qβ particle was the maximum labeling density that could be achieved without significant sign of insoluble aggregate formation. The detectable fluorescence for the FNIR-Tag conjugates was significantly higher than that of the IR-800CW conjugates at both 2 and 24 h (Figure 6D), and the signal for the IR-800CW conjugates was not detectable at 24 h even when a high threshold was used. Although preliminary, these data suggest that FNIR-Tag allows for greater labeling densities, which subsequently enables the sensitive imaging of biotherapeutic molecules at much lower doses than can be achieved using IR-800CW.

CONCLUSION

We developed a novel NIR fluorophore, FNIR-Tag, that has excellent properties for biomolecule labeling and *in vivo* imaging applications. The net-neutral zwitterionic dye appears to circumvent the issue of H-aggregation upon biomolecule conjugation within a reasonable range of labeling density. Reduced aggregation dramatically increases NIR emission of the corresponding mAb conjugates relative to the extensively used persulfonated fluorophore IR-800CW. Antibody conjugates of FNIR-Tag exhibit superior tumor uptake, reduced liver uptake, and enhanced brightness when compared to a similarly labeled IR-800CW conjugate in an *in vivo* imaging study in mice bearing EGFR+ tumors. We also observed that modification with IR-800CW induced irreversible aggregation above a moderate degree of labeling. The advantages of the FNIR-Tag conjugates were also apparent from preliminary *in vitro* and *in vivo* studies, as they proved significantly brighter in cellular association studies, and their stability at high degrees of modification allowed for superior detection in mice at a lower overall dose compared to VLPs modified with IR-800CW. In total, these studies introduce a new solution to the long-standing problem of NIR fluorophore aggregation. These efforts also illustrate that the charge and placement of peripheral substituents can play a critical role in fluorophore function and provide promising fluorophores for a range of applications where high-density labeling is desirable.

ASSOCIATED CONTENT

Supporting Information

The Supporting Information is available free of charge on the ACS Publications website at DOI: 10.1021/acschembio.9b00122.

Materials and methods, experimental procedures, and additional results (PDF)

AUTHOR INFORMATION

Corresponding Author

*E-mail: martin.schnermann@nih.gov.

ORCID

Michael P. Luciano: 0000-0002-1996-1587

M. G. Finn: 0000-0001-8247-3108

Martin J. Schnermann: 0000-0002-0503-0116

Notes

The authors declare no competing financial interest.

ACKNOWLEDGMENTS

This work was supported by the Intramural Research Program of the National Institutes of Health (NIH), NCI-CCR, NIH award GM101421, and the National Science Foundation (predoctoral research fellowship to S.N.C.). Dr. Luke Lavis, Janelia Research Campus, Howard Hughes Medical Institute, is acknowledged for assistance with instrumentation for fluorescence quantum yield determination.

REFERENCES

(1) Rosenthal, E. L., Warram, J. M., Bland, K. I., and Zinn, K. R. (2015) The status of contemporary image-guided modalities in oncologic surgery. *Ann. Surg. 261*, 46−55.

(2) Garland, M., Yim, J. J., and Bogyo, M. (2016) A Bright Future for Precision Medicine: Advances in Fluorescent Chemical Probe Design and Their Clinical Application. *Cell Chem. Biol. 23*, 122−136.

(3) Pauli, J., Grabolle, M., Brehm, R., Spieles, M., Hamann, F. M., Wenzel, M., Hilger, I., and Resch-Genger, U. (2011) Suitable labels for molecular imaging–influence of dye structure and hydrophilicity on the spectroscopic properties of IgG conjugates. *Bioconjugate Chem. 22*, 1298−1308.

(4) Ghosh, S. C., Hernandez Vargas, S., Rodriguez, M., Kossatz, S., Voss, J., Carmon, K. S., Reiner, T., Schonbrunn, A., and Azhdarinia, A. (2017) Synthesis of a Fluorescently Labeled (68)Ga-DOTA-TOC Analog for Somatostatin Receptor Targeting. *ACS Med. Chem. Lett. 8*, 720−725.

DOI: 10.1021/acschembio.9b00122
ACS Chem. Biol. 2019, 14, 934−940

(5) Kovar, J. L., Simpson, M. A., Schutz-Geschwender, A., and Olive, D. M. (2007) A systematic approach to the development of fluorescent contrast agents for optical imaging of mouse cancer models. *Anal. Biochem. 367*, 1−12.
(6) Cilliers, C., Nessler, I., Christodolu, N., and Thurber, G. M. (2017) Tracking Antibody Distribution with Near-Infrared Fluorescent Dyes: Impact of Dye Structure and Degree of Labeling on Plasma Clearance. *Mol. Pharmaceutics 14*, 1623−1633.
(7) Cohen, R., Vugts, D. J., Stigter-van Walsum, M., Visser, G. W., and van Dongen, G. A. (2013) Inert coupling of IRDye800CW and zirconium-89 to monoclonal antibodies for single- or dual-mode fluorescence and PET imaging. *Nat. Protoc. 8*, 1010−1018.
(8) Randolph, J. B., and Waggoner, A. S. (1997) Stability, specificity and fluorescence brightness of multiply-labeled fluorescent DNA probes. *Nucleic Acids Res. 25*, 2923−2929.
(9) Mujumdar, R. B., Ernst, L. A., Mujumdar, S. R., and Waggoner, A. S. (1989) Cyanine dye labeling reagents containing isothiocyanate groups. *Cytometry 10*, 11−19.
(10) Mujumdar, R. B., Ernst, L. A., Mujumdar, S. R., Lewis, C. J., and Waggoner, A. S. (1993) Cyanine dye labeling reagents: sulfoindocyanine succinimidyl esters. *Bioconjugate Chem. 4*, 105−111.
(11) Mujumdar, S. R., Mujumdar, R. B., Grant, C. M., and Waggoner, A. S. (1996) Cyanine-labeling reagents: Sulfobenzindocyanine succinimidyl esters. *Bioconjugate Chem. 7*, 356−362.
(12) Rosenthal, E. L., Warram, J. M., de Boer, E., Chung, T. K., Korb, M. L., Brandwein-Gensler, M., Strong, T. V., Schmalbach, C. E., Morlandt, A. B., Agarwal, G., Hartman, Y. E., Carroll, W. R., Richman, J. S., Clemons, L. K., Nabell, L. M., and Zinn, K. R. (2015) Safety and Tumor Specificity of Cetuximab-IRDye800 for Surgical Navigation in Head and Neck Cancer. *Clin. Cancer Res. 21*, 3658−3666.
(13) Hoogstins, C. E., Tummers, Q. R., Gaarenstroom, K. N., de Kroon, C. D., Trimbos, J. B., Bosse, T., Smit, V. T., Vuyk, J., van de Velde, C. J., Cohen, A. F., Low, P. S., Burggraaf, J., and Vahrmeijer, A. L. (2016) A Novel Tumor-Specific Agent for Intraoperative Near-Infrared Fluorescence Imaging: A Translational Study in Healthy Volunteers and Patients with Ovarian Cancer. *Clin. Cancer Res. 22*, 2929−2938.
(14) Gao, R. W., Teraphongphom, N., de Boer, E., van den Berg, N. S., Divi, V., Kaplan, M. J., Oberhelman, N. J., Hong, S. S., Capes, E., Colevas, A. D., Warram, J. M., and Rosenthal, E. L. (2018) Safety of panitumumab-IRDye800CW and cetuximab-IRDye800CW for fluorescence-guided surgical navigation in head and neck cancers. *Theranostics 8*, 2488−2495.
(15) Gorka, A. P., and Schnermann, M. J. (2016) Harnessing cyanine photooxidation: from slowing photobleaching to near-IR uncaging. *Curr. Opin. Chem. Biol. 33*, 117−125.
(16) Michie, M. S., Gotz, R., Franke, C., Bowler, M., Kumari, N., Magidson, V., Levitus, M., Loncarek, J., Sauer, M., and Schnermann, M. J. (2017) Cyanine Conformational Restraint in the Far-Red Range. *J. Am. Chem. Soc. 139*, 12406−12409.
(17) Gorka, A. P., Nani, R. R., and Schnermann, M. J. (2018) Harnessing Cyanine Reactivity for Optical Imaging and Drug Delivery. *Acc. Chem. Res. 51*, 3226−3235.
(18) Nani, R. R., Shaum, J. B., Gorka, A. P., and Schnermann, M. J. (2015) Electrophile-integrating Smiles rearrangement provides previously inaccessible C4′-O-alkyl heptamethine cyanine fluorophores. *Org. Lett. 17*, 302−305.
(19) Gorka, A. P., Nani, R. R., and Schnermann, M. J. (2015) Cyanine polyene reactivity: scope and biomedical applications. *Org. Biomol. Chem. 13*, 7584−7598.
(20) Cha, J., Nani, R. R., Luciano, M. P., Kline, G., Broch, A., Kim, K., Namgoong, J. M., Kulkarni, R. A., Meier, J. L., Kim, P., and Schnermann, M. J. (2018) A chemically stable fluorescent marker of the ureter. *Bioorg. Med. Chem. Lett. 28*, 2741−2745.
(21) Usama, S. M., Lin, C. M., and Burgess, K. (2018) On the Mechanisms of Uptake of Tumor-Seeking Cyanine Dyes. *Bioconjugate Chem. 29*, 3886−3895.
(22) Sato, K., Gorka, A. P., Nagaya, T., Michie, M. S., Nakamura, Y., Nani, R. R., Coble, V. L., Vasalatiy, O. V., Swenson, R. E., Choyke, P. L., Schnermann, M. J., and Kobayashi, H. (2016) Effect of charge localization on the in vivo optical imaging properties of near-infrared cyanine dye/monoclonal antibody conjugates. *Mol. BioSyst. 12*, 3046−3056.
(23) Sato, K., Nagaya, T., Nakamura, Y., Harada, T., Nani, R. R., Shaum, J. B., Gorka, A. P., Kim, I., Paik, C. H., Choyke, P. L., Schnermann, M. J., and Kobayashi, H. (2015) Impact of C4′-O-Alkyl Linker on in Vivo Pharmacokinetics of Near-Infrared Cyanine/Monoclonal Antibody Conjugates. *Mol. Pharmaceutics 12*, 3303−3311.
(24) Choi, H. S., Gibbs, S. L., Lee, J. H., Kim, S. H., Ashitate, Y., Liu, F. B., Hyun, H., Park, G., Xie, Y., Bae, S., Henary, M., and Frangioni, J. V. (2013) Targeted zwitterionic near-infrared fluorophores for improved optical imaging. *Nat. Biotechnol. 31*, 148−153.
(25) Choi, H. S., Nasr, K., Alyabyev, S., Feith, D., Lee, J. H., Kim, S. H., Ashitate, Y., Hyun, H., Patonay, G., Strekowski, L., Henary, M., and Frangioni, J. V. (2011) Synthesis and in vivo fate of zwitterionic near-infrared fluorophores. *Angew. Chem., Int. Ed. 50*, 6258−6263.
(26) Hyun, H., Henary, M., Gao, T., Narayana, L., Owens, E. A., Lee, J. H., Park, G., Wada, H., Ashitate, Y., Frangioni, J. V., and Choi, H. S. (2016) 700-nm Zwitterionic Near-Infrared Fluorophores for Dual-Channel Image-Guided Surgery. *Mol. Imaging Biol. 18*, 52.
(27) Su, D. D., Teoh, C. L., Samanta, A., Kang, N. Y., Park, S. J., and Chang, Y. T. (2015) The development of a highly photostable and chemically stable zwitterionic near-infrared dye for imaging applications. *Chem. Commun. 51*, 3989−3992.
(28) Yang, Z., Usama, S. M., Li, F., Burgess, K., and Li, Z. (2018) A zwitterionic near-infrared dye linked TrkC targeting agent for imaging metastatic breast cancer. *MedChemComm 9*, 1754−1760.
(29) Sato, K., Gorka, A. P., Nagaya, T., Michie, M. S., Nani, R. R., Nakamura, Y., Coble, V. L., Vasalatiy, O. V., Swenson, R. E., Choyke, P. L., Schnermann, M. J., and Kobayashi, H. (2016) Role of Fluorophore Charge on the In Vivo Optical Imaging Properties of Near-Infrared Cyanine Dye/Monoclonal Antibody Conjugates. *Bioconjugate Chem. 27*, 404.
(30) Pokorski, J. K., Hovlid, M. L., and Finn, M. G. (2011) Cell targeting with hybrid Qbeta virus-like particles displaying epidermal growth factor. *ChemBioChem 12*, 2441−2447.
(31) Pokorski, J. K., and Steinmetz, N. F. (2011) The art of engineering viral nanoparticles. *Mol. Pharmaceutics 8*, 29−43.
(32) Zhang, L., Qiu, W., Crooke, S., Li, Y., Abid, A., Xu, B., Finn, M. G., and Lin, F. (2017) Development of Autologous C5 Vaccine Nanoparticles to Reduce Intravascular Hemolysis in Vivo. *ACS Chem. Biol. 12*, 539−547.
(33) Schwarz, B., Morabito, K. M., Ruckwardt, T. J., Patterson, D. P., Avera, J., Miettinen, H. M., Graham, B. S., and Douglas, T. (2016) Viruslike Particles Encapsidating Respiratory Syncytial Virus M and M2 Proteins Induce Robust T Cell Responses. *ACS Biomater. Sci. Eng. 2*, 2324−2332.
(34) Fiedler, J. D., Higginson, C., Hovlid, M. L., Kislukhin, A. A., Castillejos, A., Manzenrieder, F., Campbell, M. G., Voss, N. R., Potter, C. S., Carragher, B., and Finn, M. G. (2012) Engineered mutations change the structure and stability of a virus-like particle. *Biomacromolecules 13*, 2339−2348.
(35) Prasuhn, D. E., Jr., Singh, P., Strable, E., Brown, S., Manchester, M., and Finn, M. G. (2008) Plasma clearance of bacteriophage Qbeta particles as a function of surface charge. *J. Am. Chem. Soc. 130*, 1328−1334.

DOI: 10.1021/acschembio.9b00122
ACS Chem. Biol. 2019, 14, 934−940